THE JOURNAL OF BIOLOGICAL CHEMISTRY VOL. 285, NO. 51, pp. 39790–39800, December 17, 2010

Gating of a G protein-sensitive Mammalian Kir3.1 Prokaryotic Kir Channel Chimera in Planar Lipid Bilayers*[S]

Received for publication, June 3, 2010, and in revised form, September 13, 2010 Published, JBC Papers in Press, October 11, 2010, DOI 10.1074/jbc.M110.151373

Edgar Leal-Pinto[‡1], Yacob Gómez-Llorente[§1,2], Shobana Sundaram[‡1], Qiong-Yao Tang[‡], Tatyana Ivanova-Nikolova[‡], Rahul Mahajan[‡3], Lia Baki[‡], Zhe Zhang[‡], Jose Chavez[§], Iban Ubarretxena-Belandia[§4], and Diomedes E. Logothetis[‡5]

From the [‡]Department of Physiology and Biophysics, School of Medicine, Virginia Commonwealth University, Richmond, Virginia 23298 and the [§]Department of Structural and Chemical Biology, Mount Sinai School of Medicine, New York, New York 10029

Kir3 channels control heart rate and neuronal excitability through GTP-binding (G) protein and phosphoinositide signaling pathways. These channels were the first characterized effectors of the $\beta\gamma$ subunits of G proteins. Because we currently lack structures of complexes between G proteins and Kir3 channels, their interactions leading to modulation of channel function are not well understood. The recent crystal structure of a chimera between the cytosolic domain of a mammalian Kir3.1 and the transmembrane region of a prokaryotic KirBac1.3 (Kir3.1 chimera) has provided invaluable structural insight. However, it was not known whether this chimera could form functional K^+ channels. Here, we achieved the functional reconstitution of purified Kir3.1 chimera in planar lipid bilayers. The chimera behaved like a *bona fide* Kir channel displaying an absolute requirement for PIP_2 and Mg^{2+}-dependent inward rectification. The channel could also be blocked by external tertiapin Q. The three-dimensional reconstruction of the chimera by single particle electron microscopy revealed a structure consistent with the crystal structure. Channel activity could be stimulated by ethanol and activated G proteins. Remarkably, the presence of both activated Gα and G$\beta\gamma$ subunits was required for gating of the channel. These results confirm the Kir3.1 chimera as a valid structural and functional model of Kir3 channels.

GTP-binding (G)[6] protein-sensitive potassium (K^+) channels comprise the third subfamily of inwardly rectifying (Kir) channels, so called as they conduct more current in the inward than outward direction. Like all Kir family members, Kir3 channels depend on phosphoinositides to maintain their activity (1–3). Kir3 channels are unique among other Kir members in that their activity is stimulated by the $\beta\gamma$ subunits of G proteins (G$\beta\gamma$) (4, 5). Indeed, a wide variety of G protein-coupled receptors activate Kir3 channels, including the M_2-muscarinic, opioid, 5-HT serotonin, A_1-adenosine, α_2-adrenergic, D_2-dopamine, and $GABA_B$ receptors (6). Kir3 channels play an important role in human physiology as they can control heart rate and neuronal excitability (7).

A number of comprehensive Kir reviews summarize numerous background studies on this type of K^+ channels (*e.g.* Refs. 7, 8). Four mammalian Kir3 members have been identified (Kir3.1–3.4) (9–12). Kir channels consist of a pore (P) region flanked by two transmembrane domains (M1 and M2). A recent crystallographic structure of Kir2.2 (13) confirmed a similar architecture for the transmembrane portion of a mammalian Kir channel compared with bacterial channels, such as the KcsA, KirBac1.1, and KirBac3.1 (14–16). High resolution structures of a chimera (hereafter referred to as the Kir3.1 chimera) between the cytosolic region of Kir3.1 and the transmembrane region of a prokaryotic Kir channel (KirBac1.3) have indeed captured one of the putative cytosolic gates (the G-loop gate) in two states, seemingly "open" and "closed" (17). Structures of complexes of Kir3 channel intracellular domains (18–20) or the Kir3.1 chimera with the G$\beta\gamma$ subunits have not yet been elucidated, presumably because of their low stability.

Kir3.1 channels do not form functional homomers and they localize poorly to the cell surface (*e.g.* Ref. 21). Yet, they potentiate the activity of other Kir3 channels upon assembly into heteromeric complexes (*e.g.* Refs.12, 22). Kir3 channels, other than Kir3.1, also exist as homotetramers (*e.g.* Kir3.2 or Kir3.4) (11, 23), albeit exhibiting lower activity than when found in heteromeric complexes with Kir3.1. Specific point mutations in a pore helix position of Kir3.1 (F137S or Kir3.1*) and Kir3.4 (S143T) have yielded potentiated homomeric currents with qualitatively similar properties to the wild-type heteromeric Kir3.1/3.4 currents (23, 24). Kir3 channels are highly expressed in heart (Kir3.1, Kir3.4) and brain (Kir3.1, Kir3.2, Kir3.3).

Phosphoinositides regulate the activity of many different ion channels and transporters (*e.g.* 25–26). Phosphoinositide dependence of Kir channels has been studied extensively (25–

* This work was supported, in whole or in part, by National Institutes of Health Grant R01 HL59949 (to D. E. L.) and National Science Foundation Grant MCB-0546087 (to I. U.-B.).
[S] The on-line version of this article (available at http://www.jbc.org) contains supplemental Figs. S1–S5.
[1] These authors contributed equally to this work.
[2] Supported by a postdoctoral fellowship from the Ministerio de Educacion y Ciencia.
[3] Supported by an National Institutes of Health F30 award.
[4] To whom correspondence may be addressed: Dept. of Structural and Chemical Biology, Mount Sinai School of Medicine, New York, NY 10029. E-mail: Iban.Ubarretxena@mssm.edu.
[5] To whom correspondence may be addressed: Dept. of Physiology and Biophysics, VCU School of Medicine, Richmond, VA 23298. E-mail: delogothetis@vcu.edu.
[6] The abbreviations used are: G, GTP-binding; PIP_2, phosphatidylinositol 4,5-bisphosphate; DDM, dodecyl maltoside; GTPγS, guanosine 5′-3-*O*-(thio)triphosphate; EM, electron microscopy; PL, proteoliposomes; PE, phosphatidylethanolamine; PS, phosphatidylserine; FSC, Fourier shell correlation.

27). A model emerging from such studies proposes that opening of the cytosolic gates occurs as the cytosolic domains of Kir channels get tethered to the plasma membrane by virtue of electrostatic interactions between the acidic phosphoinositides and basic binding pockets on the channel surface near the inner leaflet of the lipid bilayer (26, 28). High affinity of channel-PIP_2 interactions correlates strongly with high channel activity (29). It has been suggested that channel-PIP_2 interactions affect the cytosolic G-loop gate (19) and that mutations that cause disease alter channel-PIP_2 interactions (25, 29). Furthermore ethanol has been shown to activate Kir3 channels (6, 7).

The structure of the Kir3.1 chimera (17) is the first high resolution Kir3 structure that contains both cytosolic and transmembrane channel domains. The chimera contains the Kir3.1 residues Lys^{41}–Trp^{82} (N terminus) and Phe^{181}–Leu^{371} (bottom of M2 and C terminus) and the KirBac1.3 residues Phe^{45}–Ala^{127} (transmembrane domains and extracellular loops). Thus, the chimera is missing the transmembrane domains (Asn^{83}–Met^{180}) and the last 129 C-terminal residues (Ile^{372}–Thr^{501}) of Kir3.1. The lack of functional expression or reconstitution of activity of this chimeric channel casted doubt as to its usefulness in being utilized as a model for Kir3 structure and function studies.

Here, we aimed to functionally reconstitute the purified Kir3.1 chimera in planar lipid bilayers and to test its sensitivity to molecules that modulate Kir3 activity, such as phosphoinositides, ethanol and G proteins. A three-dimensional reconstruction of the Kir3.1 chimera by single particle electron microscopy was consistent with the crystal structure. Purified Kir3.1 chimera displayed activity only in the presence of phosphatidylinositol 4,5-bisphosphate (PIP_2). Ethanol stimulated the activity of the Kir3.1 chimera, consistent with its effect on wild-type Kir3 currents. Interestingly, the activity of the Kir3.1 chimera was inhibited rather than stimulated by nanomolar concentrations of $G\beta\gamma$ or $G\alpha$-GDP or $G\alpha$-GTPγS. Yet, activity of the Kir3.1 chimera was stimulated in the presence of both activated G-protein subunits (*i.e.* $G\alpha$-GTPγS and $G\beta\gamma$). Such stimulation recovered approximately half of the PIP_2-induced activity that had been inhibited by the individual G protein subunits or the heterotrimeric complex. These results pave the way for future electrophysiology and structural studies of the Kir3.1 chimera in complex with the G protein subunits aimed at understanding the molecular basis of Kir3 channel regulation.

EXPERIMENTAL PROCEDURES

Expression and Purification of the Kir3.1 Chimera—The expression and purification of the Kir3.1 chimera was carried out following a previously described protocol (17) with the following modifications: 1) Following incubation with thrombin to remove the His tag the sample was run over a high-affinity cobalt resin (Clontech) for the second time to eliminate uncleaved material and impurities. 2) Size-exclusion chromatography was carried out using a Sephacryl S-200 gel filtration column equilibrated with buffer (8 mM Bis-Tris, pH 6.5, 120 mM KCl, 3 mM DTT, and 5 mM DDM) containing the detergent dodecyl maltoside (DDM). The identity of the Kir3.1 chimera was confirmed by in-gel digestion and mass spectrometry. The yield was ~0.5 mg of pure Kir3.1 chimera per liter of *Escherichia coli* culture.

Electron Microscopy—The Kir3.1 chimera that eluted in peak B (supplemental Fig. S1*A*) was diluted (1/20) in gel filtration buffer. A 2-μl aliquot of the dilution was adsorbed onto glow-discharged carbon-coated copper grids, and negatively stained with 2% uranyl acetate. The specimen was imaged in a Jeol 2100F FEG transmission electron microscope at 200 kV under low dose conditions, using a 2k × 2k pixel CCD camera at the equivalent calibrated magnification of 63,450. To avoid biases generated during manual particle selection, we employed a strategy that involves: automated particle selection (30), followed by statistical analysis, alignment and classification (31, 32). An initial dataset of 51,000 particles was automatically selected from 130 CCD images using EMAN (30). The software Xmipp (31, 32) was employed to extract particles in 64 × 64 images, to normalize them and to perform statistical analysis. Following normalization ~5% of the initial images were discarded using purely statistical criteria based on the standard deviation of the dataset. The contrast transfer function of the images was estimated using CTFFIND3 (33) and corrected using Bsoft (34). Subsequently, the particles were grouped into 24 different defocus groups to perform classification and heterogeneity analysis. Alignment of images, two-dimensional and three-dimensional maximum likelihood classification, and reconstruction were performed using Xmipp. To obtain representative families of the heterogeneity present in the specimen, we carried out five successive rounds of MLF2D (multireference two-dimensional alignment using maximum-likelihood in Fourier space), a maximum likelihood algorithm included in the Xmipp package (31, 32). During this process, particle images with an irregular background, close neighbors, overlapping particles and aggregates were discarded to yield a homogeneous dataset of 19,300 particles. Heterogeneity analysis and three-dimensional reconstruction was carried out using MLF3D (35). To this end, an initial volume was generated by the common lines method using EMAN and without imposing any symmetry. This volume was then filtered to a resolution of 80 Å, and its gray scale corrected according to the protocol recommended by the developers of MLF3D. From this model, 3 initial seeds were generated (using different subsets from the 19,300 particle dataset) to serve as initial volumes for MLF3D. Following 25 iterations, in which no symmetry was imposed, the two most populated volumes (containing 52 and 34% of the particles) were used to generate 4 new initial seeds for a new round of MLF3D. The resulting four volumes were very similar and their back-projections were comparable to reference-free average classes solved by MLF2D. The first volume, containing 35% of the particle images (6,900 out of 19,300) and an estimated resolution of 24 Å, was selected to calculate the final reconstruction by imposing 4-fold symmetry around the *z* axis. The 0.5 criterion of the Fourier shell correlation (FSC) was employed to estimate the resolution of the final map.

Reconstitution into Planar Lipid Bilayers—Bilayer experiments were performed as described (36, 37). Briefly, puri-

fied Kir3.1 chimera was used to form proteoliposomes (PLs) by sonicating the purified protein with a 1:1 mixture of bovine brain phosphatidylethanolamine (PE: 10 mg/ml) and phosphatidylserine (PS: 10 mg/ml). The experimental apparatus consisted of two 1-ml buffer chambers separated by a Teflon film that contained a single 50–100-μm hole. A lipid bilayer was formed by "painting" the hole with a 1:1 mixture of PE and PS dissolved in *n*-decane to a final concentration of 50 μg/ml. This resulted in formation of a high-resistance seal between the two cups. For these studies, the *Cis* side was defined as the chamber connected to the voltage-holding electrode, and all voltages are referenced to the *Trans* (ground) chamber. Stability of the bilayer was determined by clamping the voltage at various levels. If a resistance was >100 GΩ, the noise <0.2 pA, and the bilayer was stable 5 μl aliquots of PLs containing the Kir3.1 chimera were added to the *Trans* side of the chamber and stirred for 5 min. When channel activity was observed, PLs were washed from the *Trans* chamber to limit further channel incorporation. The orientation of the Kir3.1 chimera insertion was with the intracellular surface facing the *Cis* side of the bilayer. We attribute our high success of channel insertion at the appropriate orientation to the asymmetry of the lipids used (38). Records were filtered at 10 kHz, unless otherwise indicated. Channel events with an open time greater than 2.0 ms and a noise level at the open state less than two times the background noise were further filtered at 1 kHz for further analysis (see below). All experiments were performed with either symmetrical buffered solutions or with ionic gradients to examine channel selectivity. Exact composition of solutions used in each experiment is described below. For all of the experiments (Kir3.1 chimera or oocytes membranes) the solutions were similar containing in mM: 150 KCl, 1 $CaCl_2$, 1 $MgCl_2$, 1% Chaps, 10 Tris-Hepes, pH 7.4. The solutions were symmetrical in both sides of the chamber unless otherwise indicated.

Electrophysiological Data and Statistical Analysis—The bilayer channel events were analyzed using the Clampfit module (version 9.2.1.9) of pClamp (Axon Inc.). The software determines the valid channel transitions (*i.e.* openings and closings), based on 50% threshold crossing methods. If multiple channel events are observed in a single patch/recording, the total number of functional channels (N) in the patch can be estimated from the number of peaks in the all point amplitude histogram. In such cases, the product of number of channels (N) and the open probability (P_o) can be used to measure the channel activity in the patch. In the records shown in Fig. 5, *C–F*, NP_o was obtained in 10 s sequential intervals throughout the experiment. For each condition, the reagent indicated was added to either the *Cis* or *Trans* side of the bilayer as indicated and the resulting NP_o was normalized to the corresponding NP_o for PIP_2. Percent NP_o data were pooled together in the summary graphs shown in 5*D*, *F*, which plot mean ± S.E. values. Statistical significance shown for these plots was obtained using one-way ANOVA analysis in MicroCal Origin 7.5.

RESULTS

Electron Microscopy and Three-dimensional Reconstruction of the Kir3.1 Channel Chimera

The Kir3.1 chimera was expressed in *E. coli* and purified (supplemental Fig. S1) in DDM, following a protocol described by Nishida *et al.* (17). To ensure that the purified protein to be employed in our electrophysiology experiments retained its tetrameric assembly and structural integrity, we performed a three-dimensional reconstruction of the chimera using single particle electron crystallography. Fig. 1*A* displays a representative field view showing abundant globular particles with a diameter of ~100 Å (see "Experimental Procedures"). The remaining subset of particle images (19,300 particles, ~38% of the initial dataset) displayed a very high correlation in terms of size and background. The reference-free class averages generated for this subset appeared as different projections from the same object (Fig. 1*B*), and displayed an enrichment of lateral orientations (supplemental Fig. S2*A*). This subset of 19,300 particle images was employed for three-dimensional reconstruction and refinement, coupled with heterogeneity analysis (35). Fig. 1*C* illustrates the reconstructed volume after applying a 4-fold symmetry parallel to the *z* axis. Back-projections of the three-dimensional reconstruction correspond closely with reference-free class averages (supplemental Fig. S2*B*), indicating consistency between the reconstructed structure and the particle dataset. The final structure (Fig. 1*C*) was determined to a resolution of 24 Å based on the 0.5 criterion of the FSC (supplemental Fig. S2*C*). Fig. 1*D* displays a cut-away view to show the fitting of the crystal structure of the Kir3.1 chimera tetramer (PDB code: 2QKS) solved by Nishida *et al.* (17).

Overall, our EM map was consistent with the x-ray structure of the tetrameric chimera, indicating that the protein employed in our experiments was indeed tetrameric. Notably, the cytoplasmic region of the x-ray structure fitted very well (manual fitting using CHIMERA (39)) within the envelope of our reconstruction. In the transmembrane region a semi-spherical additional mass could be observed likely corresponding to DDM molecules arranged concentrically around the transmembrane helices of the chimera. We note that comparable features due to bound detergent have been observed in single particle EM structures of detergent-solubilized membrane proteins both under negative stain (40) and in vitreous ice (41).

Functional Reconstitution of the Kir3.1 Chimera and Its Characteristic Properties

Unsuccessful Attempts—Nishida *et al.* (17) concluded their structural study of the Kir3.1 chimera unable to obtain functional reconstitution of this protein. They had attempted functional reconstitution in planar lipid membranes consisting of POPE:POPG lipids in a 3:1 ratio and speculated several potential reasons for the lack of function. 1) There could have been an unmet lipid requirement. 2) The chimera could have been non-functional as a homomultimer, because Kir3.1 is normally functional as a heteromultimer with other members of the Kir3 family. 3) The chimera might have lacked the

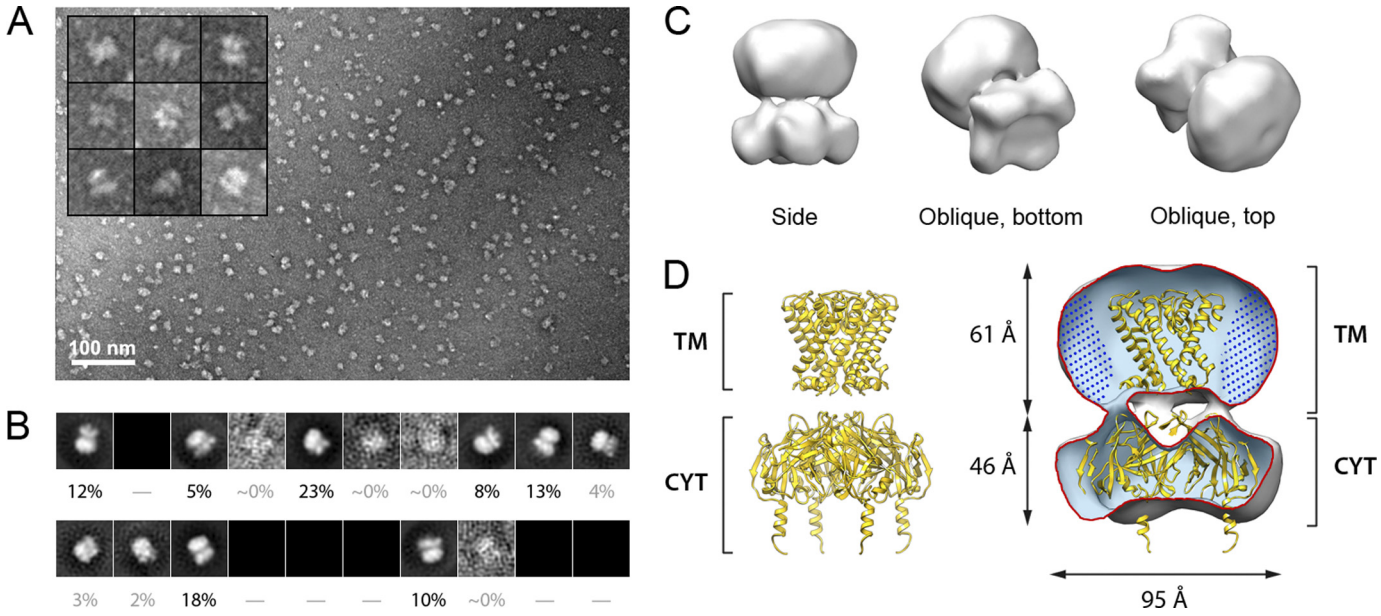

FIGURE 1. **Single particle EM of the Kir3.1 channel chimera.** *A*, representative field view of the negatively stained Kir3.1 chimera. The *inset* displays a gallery of characteristic particles. *B*, reference-free class averages produced by MLF2D, after five cycles of alignment and classification, to produce a working set of 19,300 particles. The percentage of particle images in each class is denoted. Out of 20 possible class averages, the particles in the dataset populated mainly seven classes. *C*, three-dimensional structure of the Kir3.1 chimera filtered to a resolution of 24 Å. Different views of the calculated isosurface contoured at 3 sigma are shown. *D*, fitting of the x-ray structure of the Kir3.1 channel chimera (PDB code: 2QKS) inside a cutaway of the volume. The locations of the transmembrane (*TM*) and cytoplasmic regions (*CYT*) are given. The region filled with *dots* around the TM region is suggested to correspond to DDM detergent molecules.

proper coupling between the cytoplasmic and transmembrane pores; and 4) the prokaryotic transmembrane domain of the chimera could have been problematic for functional reconstitution into the bilayer system, as single channel activity had not been demonstrated for any of the prokaryotic Kir channels.

Because Kir3.1 is found as a complex with Kir3.4 in atrial cells giving rise to K_{Ach}, we first set out to test whether the Kir3.1 chimera could be functionally expressed in *Xenopus laevis* oocytes or HEK-293 cells, either by itself or in complex with Kir3.4 subunits. Injection into *Xenopus* oocytes of the Kir3.1 chimera mRNA alone (supplemental Fig. S3, *B* and *F*) or together with Kir3.4 mRNA (supplemental Fig. S2, *D* and *F*) yielded no significantly increased currents compared with the muscarinic type 2 receptor (M_2R control) injected alone (supplemental Fig. S3, *A* and *F*) or together with twice the amount of Kir3.4 (Kir3.4 control) (supplemental Fig. S3, *C* and *F*). In contrast, co-injection of wild-type Kir3.1 and Kir3.4 mRNAs resulted in significantly higher currents than any of the homomeric subunit injections alone, consistent with previous results (supplemental Fig. S3, *E* and *F*) (12, 42).

Tagging of the C-terminal cytoplasmic tail of the Kir3.1 chimera with EGFP (Kir3.1 Chim-GFP) and transfecting HEK-293 cells, revealed lack of cell surface expression (supplemental Fig. S4*A*), similar to that previously observed with Kir3.1-GFP alone (*e.g.* 24). Even co-transfection of Kir3.4 failed to alter cell surface expression of the Kir3.1 Chim-GFP (supplemental Fig. S4*B*), in sharp contrast with Kir3.1-GFP shown previously (21). These results are consistent with the interpretation that the Kir3.1 chimera neither produces functional homomeric channels nor it localizes to the cell surface. In addition, the chimera failed to show potentiated currents when expressed together with Kir3.4 and to be localized to the cell surface, suggesting a possible failure to associate with Kir3.4. Indeed, the Kir3.1 chimera is missing the 40 amino acid residues of N-terminal end of Kir3.1 that have been shown previously to be critical for heteromeric assembly with Kir3.4 and cell surface localization (21). Following these unsuccessful attempts to attain functional expression from the Kir3.1 chimera in two different cell systems, we focused our efforts in reconstitution studies into planar lipid bilayers, exploring further the potential problems discussed by Nishida *et al.* (17).

Successful Functional Reconstitution in Planar Lipid Bilayers—Bilayer experiments were performed as previously described (36, 37). Briefly, the affinity purified Kir3.1 chimera was used to form PLs by sonicating at 80 KHz for 1 min with a 1:1 mixture of bovine brain PE (10 mg/ml) and PS (10 mg/ml). For these studies, the *Cis* (intracellular) side was defined as the chamber connected to the voltage-holding electrode and all voltages were referenced to the *Trans* (ground or extracellular) chamber. The insertion of channels in the bilayer was assessed by the presence of clear current transitions from a level of zero current (see "Experimental Procedures").

Fig. 2*A* shows that when, along with the purified Kir3.1 chimera contained in perfused PLs, diC8 phosphatidylinositol-bisphosphate (PIP_2) was added to the *Cis* but not the *Trans* side of the bilayer, clear channel activity was obtained. Addition of 50 nM of the naturally occurring arachidonyl-stearyl (AASt) PIP_2 to the *Cis* side of the bilayer resulted in ~100% channel open probability ($n = 36$). The water-soluble, eight-carbon long analog of PIP_2, diC8-PIP_2, although less effective than AASt PIP_2 (43) has proven very useful, as it allows con-

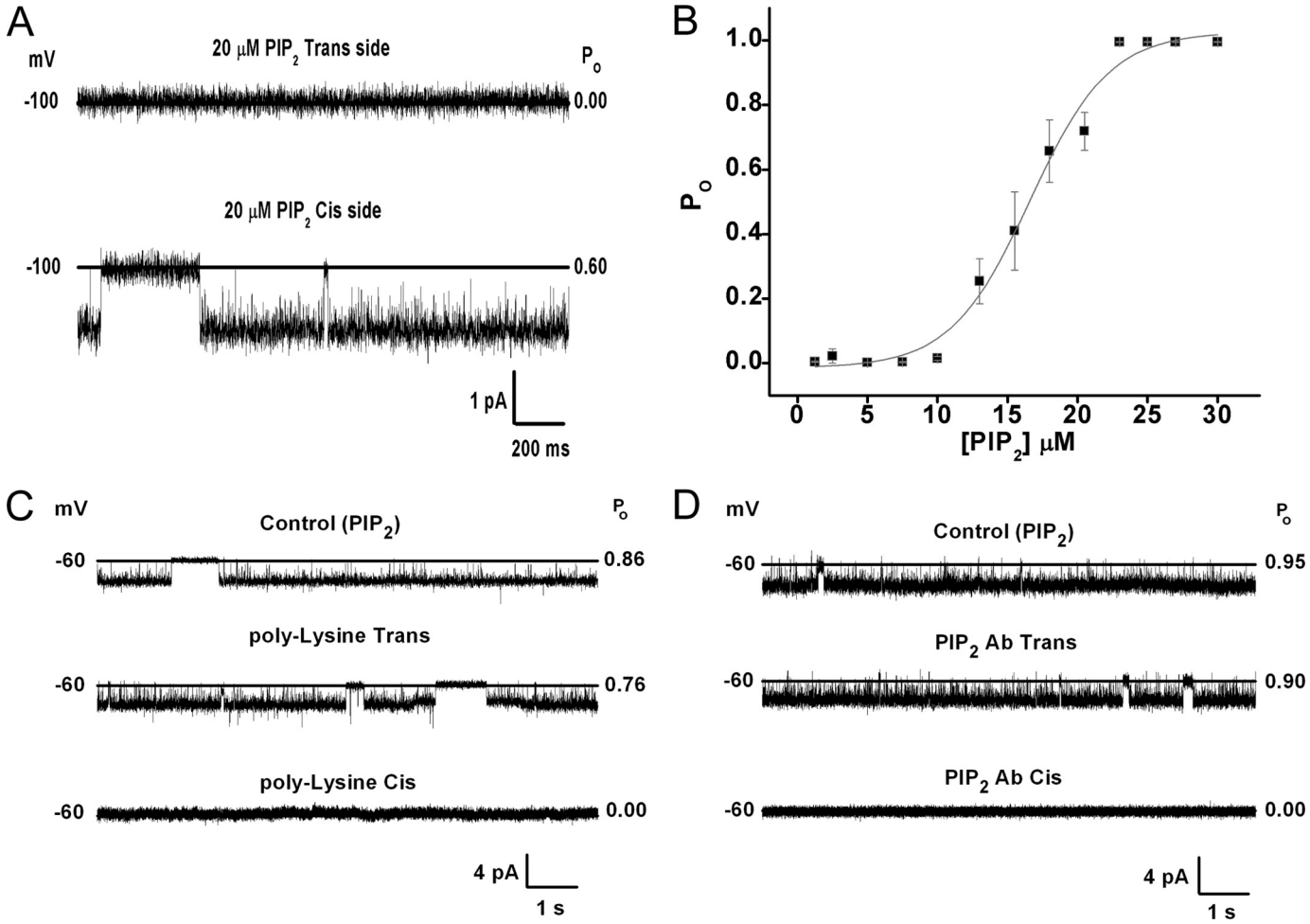

FIGURE 2. **Functional reconstitution of the Kir3.1 chimera requires PIP_2.** *A*, 2-s traces of the Kir3.1 chimera reconstituted in a planar lipid bilayer in which 20 μM diC8-PIP_2 was added from the *Trans* side (*top*) or the *Cis* side (*bottom*). *B*, dose-response curve of DiC8-PIP_2 applied from the *Cis* side. Data points represent mean ± S.E. from four experiments ran in triplicate were fitted to the equation: $y = B \times x^n/\{(k)^n + x^n\}$, where $y = P_o$; $x = [PIP_2]$; $B = 1.07 \pm 0.05$; EC_{50}, $k = 16.75 \pm 0.50$; Hill coefficient, $n = 5.54 \pm 0.77$; $chi^2 = 0.00214$. *C*, holding potential values (*left*), 10-s representative traces (*middle*), and open probability values (*right*) of the reconstituted chimera in the presence of 20 μM diC8-PIP_2. Control (*upper trace*), 300 μg/ml polylysine added to the *Trans* side (*middle trace*) or to the *Cis* side (*lower trace*), $n = 3$. *D*, holding potential values (*left*), 20-s representative traces (*center*) and open probability values (*right*) of the Kir3.1 chimera activity in the presence of 20 μM diC8-PIP_2. Control (*upper trace*), 1:200 dilution PIP_2 Ab added to the *Trans* side (*middle*) or 1:200 dilution PIP_2 Ab added to the *Cis* side, $n = 3$.

struction of dose-response relationships and estimation of relative apparent affinities of ion channels to PIP_2. The Kir3.1 chimera showed a relatively high apparent affinity for diC8-PIP_2 ($EC_{50} = 16.75 \pm 0.50$ μM) (Fig. 2*B*). In comparison, analogous experiments using inside-out patches from *Xenopus* oocytes expressing the full-length active homomer Kir3.1* yielded lower apparent affinities ($EC_{50} = 30.6 \pm 3.8$ μM, $n =$ 3–5), suggesting that the Kir3.1 chimera experiences stronger interactions with PIP_2 than Kir3.1*. Scavengers of PIP_2, such as poly-Lysine (Fig. 2*C*) or PIP_2 antibody (PIP_2 Ab, Fig. 2*D*) inhibited diC8 PIP_2-stimulated channel activity when applied to the *Cis* side but not the *Trans* side. Similar results using polylysine or PIP_2 Ab were obtained when the Kir3.1 chimera had been activated by AASt-PIP_2. These results confirmed that Nishida *et al.* were unable to functionally reconstitute the Kir3.1 chimera in lipid bilayers due to an unmet lipid requirement, namely the presence of PIP_2.

The Kir3.1 chimera exhibited biophysical properties characteristic of Kir channels. Single-channel currents showed intraburst kinetics exhibiting one closed-time ($\tau_c = 0.31$ ms) and two open-time ($\tau_{o1} = 1.6$ ms, $\tau_{o2} = 29.7$ ms) components (Fig. 3*B*) and a 29.3 + 6.7 pS unitary conductance (Fig. 3*C*). Inward rectification was obtained in the presence of intracellular Mg^{2+} (Fig. 3, *A* and *C*, *right panel*), while a linear current-voltage relationship was obtained in the absence of intracellular Mg^{2+} (Fig. 3*C*, *left panel*). 100 nM of the peptide Tertiapin Q, which blocks potently Kir3 and Kir1.1 currents (44–46), added to the *Trans* but not to the *Cis* side, inhibited the activity of the Kir3.1 chimera (Fig. 3*D*). Both the internal Mg^{2+}-dependent rectification and the external block by Tertiapin Q are defining characteristics of Kir channels.

Because Kir3 activation by ethanol is thought to result by association of the alcohol in a physical binding pocket of the channel (47), we tested the effects of ethanol on the activity of the Kir3.1 chimera. Fig. 4*A* shows a representative record, where 0.8% ethanol, a concentration shown to stimulate Kir3 currents (48, 49), stimulated the activity of the Kir3.1 chimera. The significant stimulatory effect of ethanol on Kir3.1 chimeric currents ($n = 3$) (Fig. 4*B*) is an additional functional characteristic of Kir3 channels preserved in the chimera.

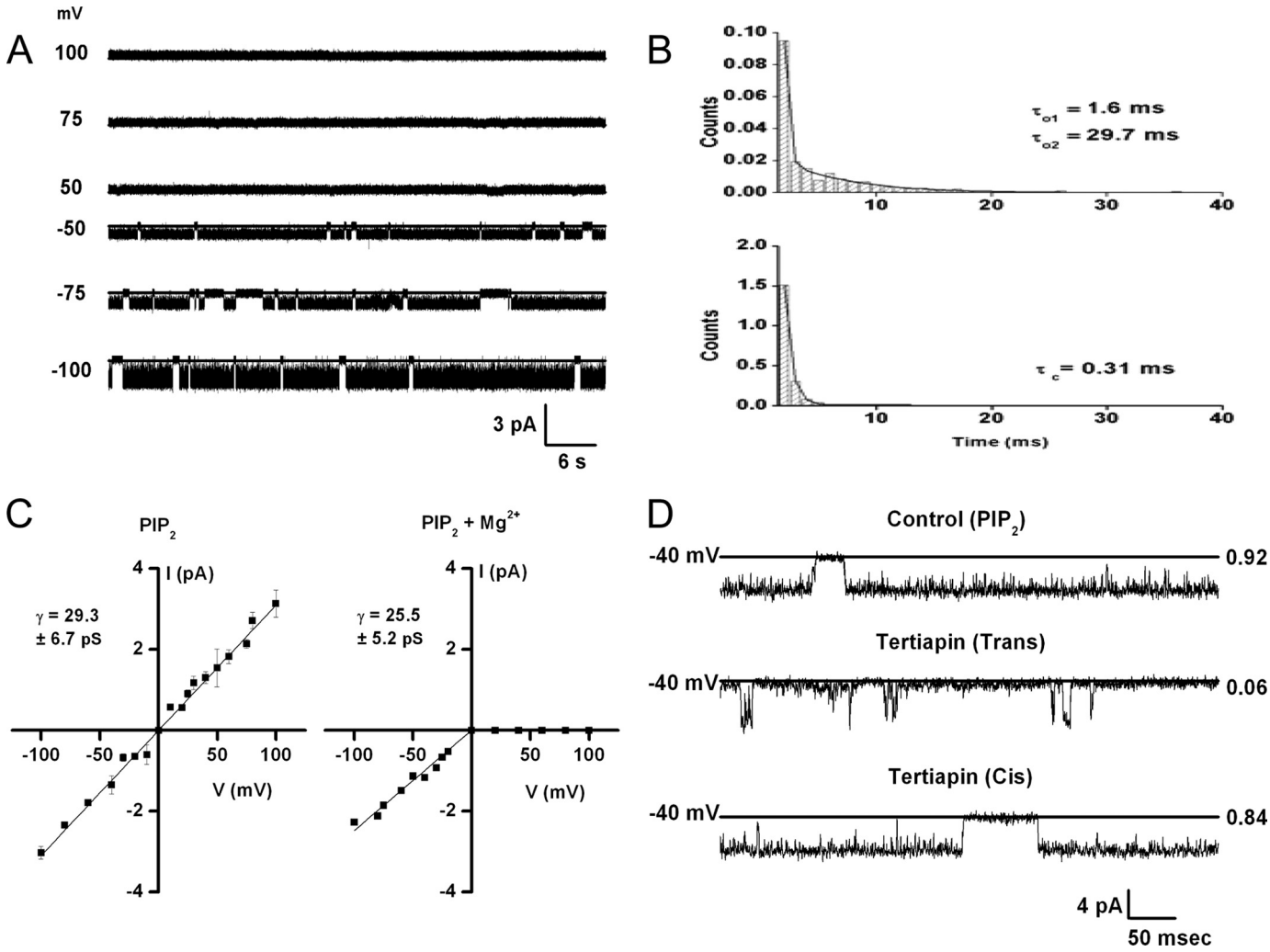

FIGURE 3. **Functional properties of Kir3.1 chimera are consistent with a Mg^{2+}-dependent inwardly rectifying channel, sensitive to block by extracellular Tertiapin Q.** *A*, 1-min representative traces of the Kir3.1 chimera reconstituted in a planar lipid bilayer. *B*, intra-burst time constants for the experiment depicted in *A*. The open-time histogram (*upper*) was best fitted with a 2-component exponential and the closed-time histogram (*lower*) was best fitted with a one-component exponential (see text and figure for values). *C*, current-voltage relationship for the Kir3.1 chimera reconstituted in the absence of Mg^{2+} (*left*) or in the presence of 1 mM Mg^{2+}, $n = 3$. *D*, 0.5 s representative traces of the chimera reconstituted under the same conditions as in *A* in the presence of 20 μM diC8-PIP_2 (control, *upper trace*) or when 100 nM Tertiapin Q was added to the *Trans* side (*middle trace*) or to the *Cis* side (*lower trace*), $n = 4$.

Another defining characteristic of Kir3 channels is their sensitivity to the $\beta\gamma$ subunits of G proteins (4). All Kir3 subunits expressed as homomers or heteromers are activated by the G$\beta\gamma$ subunits (50, 51). Nanomolar concentrations of purified G$\beta\gamma$ (Gβ1γ2) failed to stimulate the activity of the Kir3.1 chimera either in the absence of PIP_2 ($n = 7$) or in the presence of PIP_2 at concentrations that produced submaximal activity ($n = 6$). Instead, nanomolar concentrations of G$\beta\gamma$ caused an inhibition of Kir3.1 chimera channel activity by increasing the interburst intervals of unitary channel activity (Fig. 5*A*). The IC_{50} for G$\beta\gamma$ inhibition was rather high (48.97 $\pm$ 5.91 nM), possibly related to its high PIP_2 apparent affinity (Fig. 5*B*). A similar inhibition (25–30% reduction in P_o) was obtained by 16 nM G$\beta\gamma$, whether the Kir3.1 chimera was activated maximally by diC8-PIP_2 or AASt-PIP_2 ($n = 5$).

We proceeded to test whether application of purified Gα-GDP affected activity of the Kir3.1 chimera induced by 14.5 μM diC8-PIP_2. 40 nM Gαi_1-GDP caused an inhibition of channel activity (Fig. 5, *C* and *D*) similar to that caused by 42 nM G$\beta\gamma$ applied before Gα-GDP (not shown). Subsequent application of the complementary G-protein subunit did not have a significant further effect (Fig. 5, *C* and *D*, G$\beta\gamma$ following Gα-GDP). Addition of 100 μM GTPγS caused robust channel activation to levels approximately half of the PIP_2-stimulated currents. 100 nM Tertiapin Q applied to the *Trans* side of the bilayer inhibited the GTPγS-stimulated activity. This result suggested the Kir3.1 chimera could be activated by GTPγS in a manner similar to Kir3 channels expressed in native or heterologous systems (4, 12). Moreover, these experiments suggested that activation of Kir3.1 chimera by G proteins required that both subunits were in the active form.

To further assess this requirement of channel activity for both active G protein subunits, we tested whether active Gα subunits (Gα-GTPγS) affected the Kir3.1 chimera activity. Again Gα-GDP inhibited diC8 PIP_2-stimulated activity and application of GTPγS had no further effect, suggesting that

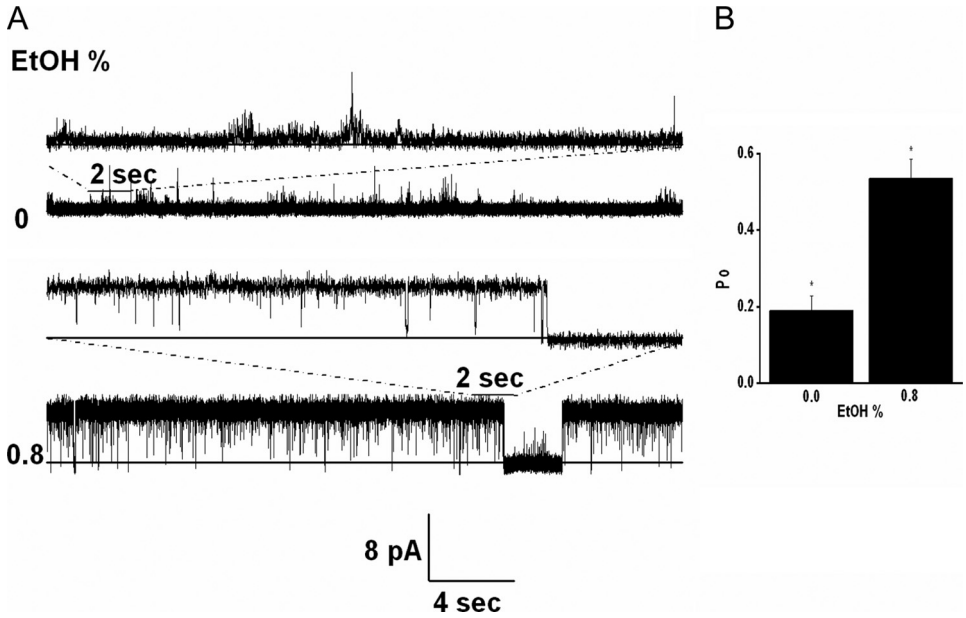

FIGURE 4. **Ethanol stimulates Kir3.1 chimeric currents.** *A*, low concentrations of diC8-PIP_2 (~5 μM) were used to give minimal channel activity in symmetrical 150 mM KCl solutions in the absence of Mg^{2+} ions. 0.8% ethanol (174 μM, *Cis* side) stimulated channel activity. The representative traces shown were collected at 10 kHz and were additionally filtered at 1 kHz. The *top trace* was recorded at +25 mV, while the *bottom trace* at +200 mV. *B*, summary data from three experiments showing channel open probability (Po) at 0% *versus* 0.8% ethanol. The data were analyzed with one way ANOVA and the means comparison, using the Bonferroni test, showed statistical significance at $p < 0.05$.

activated Gα-GTPγS was not sufficient to stimulate activity (Fig. 5, *E* and *F*). Gβγ following application of Gα-GDP and GTPγS caused significant stimulation of channel activity, again to levels of approximately half of the PIP_2-stimulated currents. Application of 100 nM Tertiapin Q to the *Trans* side of the bilayer inhibited the Gβγ-stimulated activity. These results strongly suggested that Gβγ stimulation of the activity of the Kir3.1 chimera required the co-presence of Gα-GTPγS.

To further test whether reconstitution of the G protein signaling system in planar lipid bilayers could support stimulation of Kir3 activity by Gβγ alone, we proceeded to examine the corresponding response to purified Gβγ subunits of the full-length active homomer Kir3.1* reconstituted in planar lipid bilayers. We first expressed Kir3.1* channels in *Xenopus* oocytes and prepared membrane vesicles that were reconstituted in lipid bilayers following a protocol developed by Aleksandrov *et al.* (52), for reconstitution of Kir2.1 channels. Again, we found that the presence of PIP_2 on the *Cis* side of the bilayer was critical for obtaining channel activity. Supplemental Fig. S5 shows that Kir3.1* yielded a comparable unitary conductance of 16–19 pS in Mg^{2+}-free solutions, whether recorded in inside-out patches from oocytes (supplemental Fig. S5, *A* and *B*) or reconstituted in lipid bilayers (supplemental Fig. S5, *C* and *D*).

Perfusion of inside-out patches expressing Kir3.1* with purified Gβγ subunits resulted in a clear stimulation of channel activity, whether recorded in inside-out patches from *Xenopus* oocytes (Fig. 6, *A* and *B*) or in lipid bilayers (Fig. 6, *C* and *D*). These results suggested that reconstitution of purified components of the G protein signaling system into planar lipid bilayers could be lacking a critical component present in the oocyte membranes that enables stimulation of Kir3 currents.

Gβγ stimulation of Kir3.1 channels expressed in native cells or heterologous expression systems does not require the presence of Gα-GTPγS (4). Yet in such experiments, one knows neither the identity of all molecules that are participating in the signaling complex, nor their precise functional state. Could Gβγ stimulation require that some channel subunits are bound to either Gα-GDP alone or in heterotrimeric form (Gα-GDP/Gβγ), while other subunits are bound to Gβγ alone? In other words could an excess of Gβγ subunits in the presence of Gα-GDP (or even Gα-GTPγS) stimulate the Kir3.1 chimera currents? To test for such a possibility, we repeated the experiment shown in Fig. 5, *C* and *D* but before GTPγS application, we applied an excess of Gβγ to the *Cis* side of the bilayer. Excess Gβγ did not cause a significant change in activity but GTPγS did (PIP_2 (100%); Gα-GDP (18 ± 2.9%); Gβγ, 42 nM (13 ± 1.7%); Gβγ, 84 nM (16 ± 4.7%); GTPγS (44 ± 6.2%); Tertiapin Q (10 ± 1.7%), $n = 2$). These results further reinforced the interpretation that reconstitution of purified Kir3.1 chimera and G protein subunits in planar lipid bilayers either lacked an additional component present in oocyte membranes expressing heterologous Kir3.1* or behaved somewhat differently from Kir3.1 channels. If a missing component was indeed responsible for the difference in response between the Kir3.1* and the Kir3.1 chimera, it would presumably enable Gβγ stimulation without the need of activating Gα with GTPγS.

DISCUSSION

Our study has succeeded in functionally reconstituting the Kir3.1 chimera in planar lipid bilayers and demonstrating that it behaves like a *bona fide* Kir3 channel: it displays sensitivity to PIP_2 and its scavengers as well as Mg^{2+}-dependent inward rectification from the internal membrane side, and sensitivity to

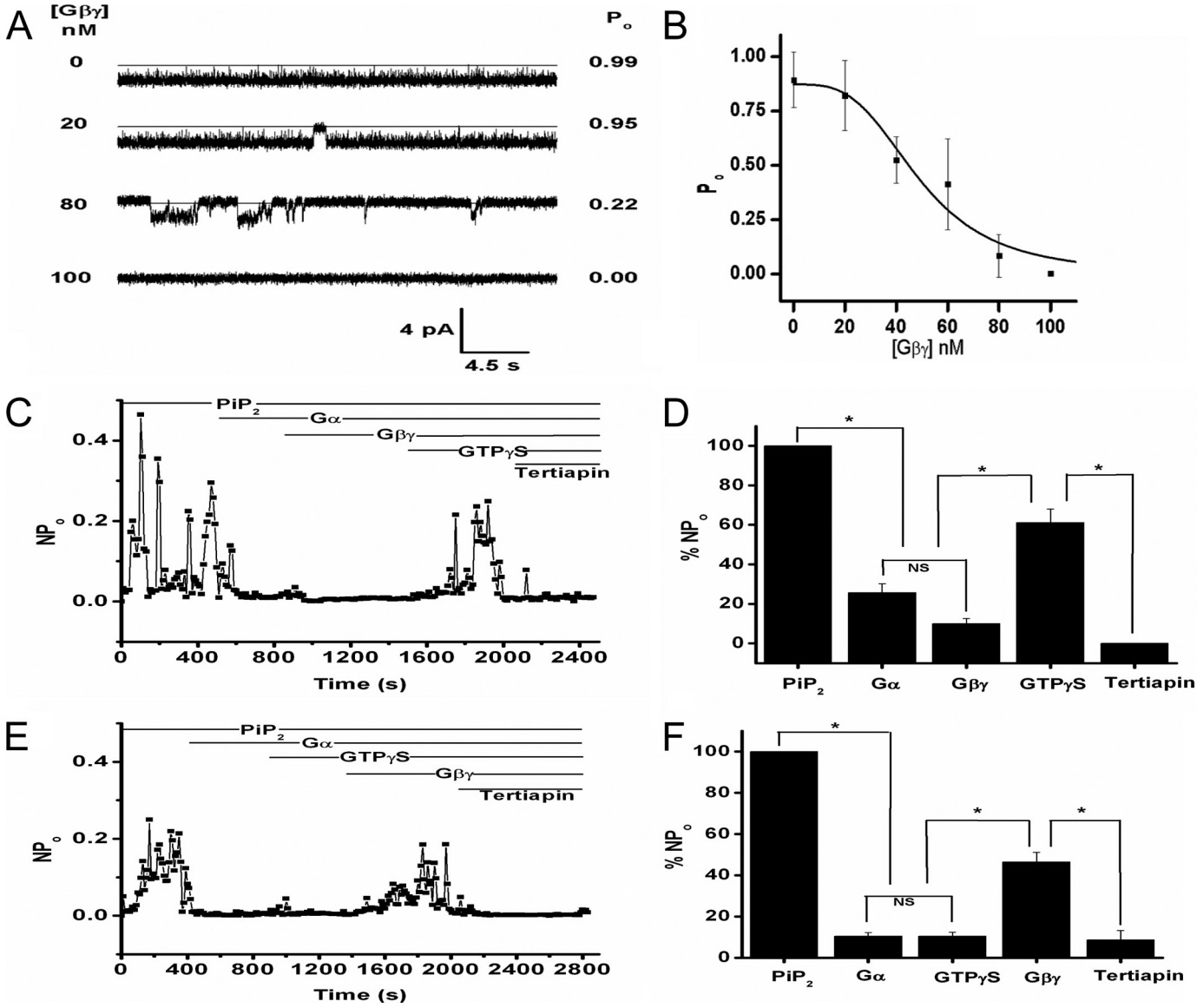

FIGURE 5. **G protein regulation of Kir3.1 chimeric currents.** *A*, G$\beta\gamma$ concentrations (*left*), 30-s representative traces (*center*) and open probability (*right*) for the chimera in the presence of 20 μM diC8-PIP2 at the G$\beta\gamma$ concentrations depicted on the *left*. The traces shown come from the same experiment and were collected at 10 kHz and were additionally filtered at 1 kHz for final analysis. *B*, G$\beta\gamma$ dose-response on the open probability of the Kir3.1 chimera ($n = 5$) reconstituted under the same conditions as in *A*. Data points were fitted to the equation: $y = B \times x^n/\{(k)^n + x^n\}$ where, $y = P_o$; $x = [G\beta\gamma]$; $B = 0.87 \pm 0.08$; EC_{50}, $k = 48.97 \pm 5.91$; Hill coefficient, $n = -3.31 \pm 1.06$; $chi^2 = 0.00865$. *C*, representative NP_o of the Kir3.1 chimera as a function of time for the entire experiment ($n = 4$). The bars at the *top* indicate the sequential addition of PIP_2 (14.5 μM), Gα-GDP (40 nM), G$\beta\gamma$ (42 nM), GTPγS (100 μM), and Tertiapin Q (100 nM). All additions except for Tertiapin were added to the *Cis* side of the chamber. *D*, bar graph of the mean NP_o ($\pm$ S.E.) for the time interval between sequential additions of PIP_2, Gα-GDP, G$\beta\gamma$, GTPγS, and Tertiapin Q ($n = 4$). *Asterisk* (*) indicates significance level of 0.05 (see "Experimental Procedures"). *E*, representative NP_o of Kir3.1 chimera as a function of time for an entire experiment ($n = 3$). The bars at the *top* indicate the sequential addition of PIP_2, Gα-GDP, GTPγS, G$\beta\gamma$, and Tertiapin Q (concentrations were similar to those indicated in *C*). All reagents except Tertiapin Q were added to the *Cis* side of the chamber. *F*, bar graph of the mean NP_o ($\pm$S.E.) for the time interval between sequential additions of PIP_2, Gα, GTPγS, G$\beta\gamma$, and Tertiapin Q ($n = 3$). All reagents except Tertiapin Q were added to the *Cis* side of the chamber. The *asterisk* (*) indicates significance level of 0.05.

block by Tertiapin Q from the external surface. Channel activity displayed an absolute requirement for PIP_2, the lack of which potentially explains previous unsuccessful attempts to functionally reconstitute it (17). At PIP_2 concentrations that produced submaximal Kir3.1 chimeric activity, ethanol stimulated channel activity consistent with its effects on wild-type Kir3 currents.

A number of unexpected findings were obtained with the G protein subunit gating of the Kir3.1 chimera. First, both Gα-GDP as well as Gα-GTPγS caused inhibition of PIP_2-stimulated currents in the complete absence of the G$\beta\gamma$ subunits. Second, and most unexpectedly, the G$\beta\gamma$ subunits also inhibited the PIP_2-stimulated Kir3.1 chimera currents. Third, the combination of Gα-GDP and G$\beta\gamma$ subunits proved incapable of stimulating channel activity, even when the G$\beta\gamma$ subunits were used in stoichiometric excess. In contrast, the fourth finding showed that G$\beta\gamma$ subunits were effective in stimulating activity of the Kir3.1 chimera in the co-presence of Gα-GTPγS. This result suggests that the Kir3.1 chimera requires both activated G protein subunits in order to have its activity stimulated (Fig. 7).

How do these results of G protein subunit effects on the Kir3.1 chimera compare with previous studies on Kir3 chan-

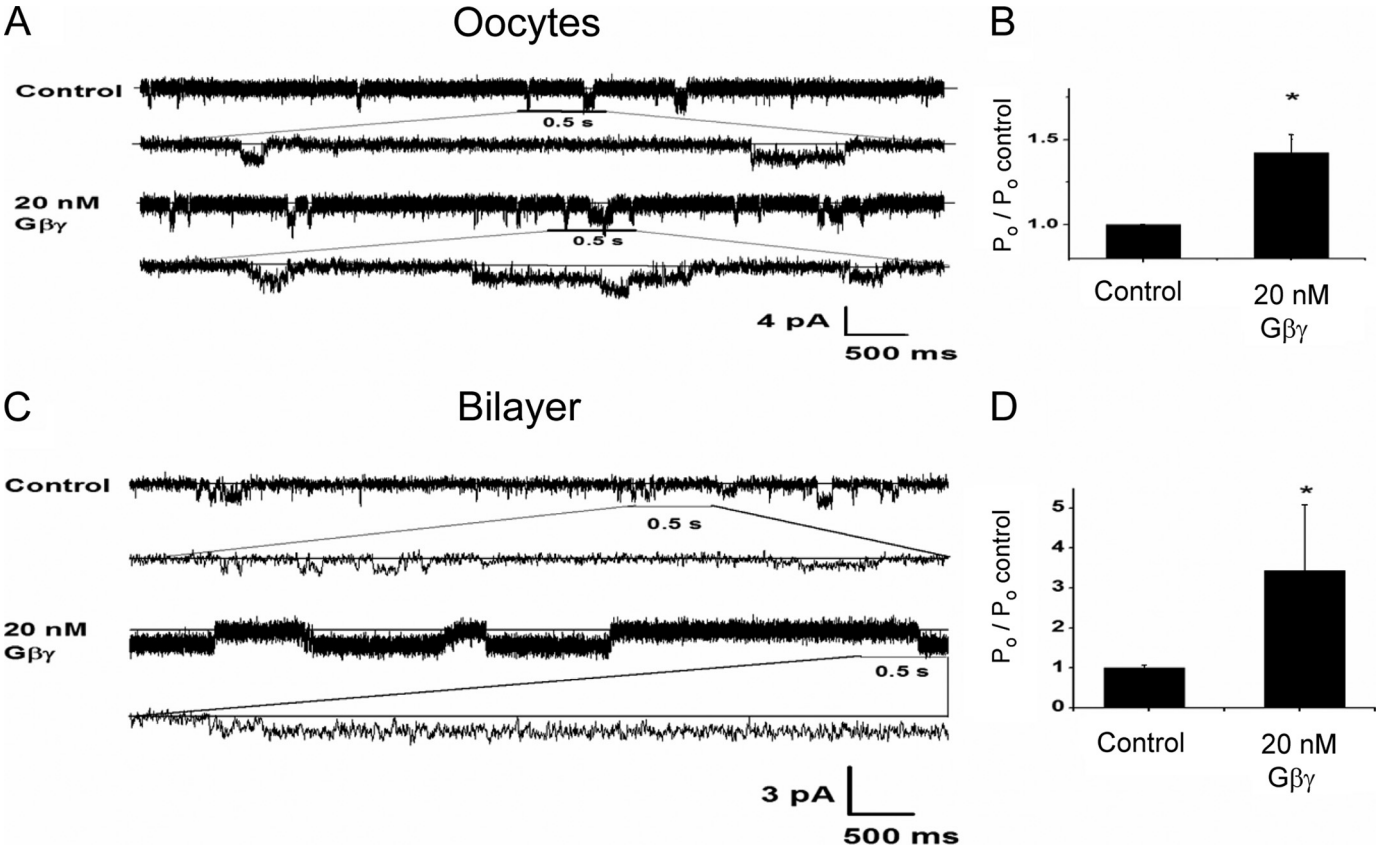

FIGURE 6. **Gβγ stimulation of Kir3.1* activity in inside-out patches or bilayers using membranes from *Xenopus* oocytes.** *A*, single-channel current traces in an inside-out patch of Kir3.1* expressed in oocytes for *Control* and after perfusion with 20 nM Gβγ in the bath. Current traces are also displayed at an expanded time scale. Membrane potential was held at −160 mV. *B*, summary data for the effect of Gβγ on Kir3.1* activity when expressed in oocytes (plotted as % of the control). The means comparison using the Student's *t* test showed statistical significance at $p < 0.01$. *C*, representative 6.5-s traces of membranes from oocytes expressing Kir3.1* reconstituted in the lipid bilayer. Similar conditions were used for oocyte membranes as was used for Kir3.1 chimera reconstitution in the absence or presence of 20 nM Gβγ on the *Cis* side. *D*, Gβγ effect on open probability (plotted as % of the control) for five experiments ran under the same conditions as in *C*. The means comparison using the Student's *t* test showed statistical significance at $p < 0.05$.

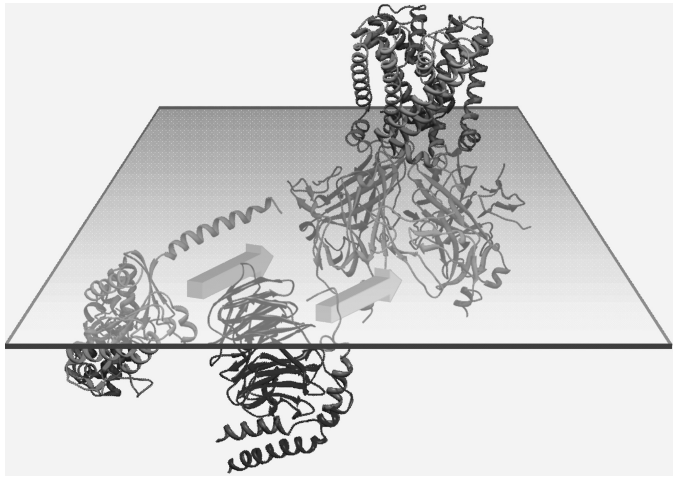

FIGURE 7. **Model of G protein subunit stimulation of the Kir3.1 chimera.** Structures of the Kir3.1 chimera, the Gα-GDP, and Gβγ, in the plane of the inner leaflet of the membrane bilayer, are shown. Both Gα-GDP and Gβγ, can interact independently or in combination to inhibit PIP_2-stimulated channel activity, while the same holds true for Gα-GTPγS. However, in the presence of Gα-GTPγS, Gβγ stimulates the activity of the Kir3.1 chimera.

nels expressed in native or heterologous cellular systems? First, Dascal and co-workers (53, 54) have argued for an inhibitory role of $G\alpha_i$ subunits (both Gα-GDP as well as Gα-GTPγS) that extends beyond their capacity to scavenge Gβγ subunits. Although there are important differences between their results and those obtained in the present studies, their claim of Gα effects independent of Gβγ is supported by the direct inhibitory effects of Gα-GDP and Gα-GTPγS on the activity of the Kir3.1 chimera in planar lipid bilayers. Second, Gβγ inhibits neuronal Ca^{2+} currents (55, 56), while it stimulates Kir3 currents. Yet in cell systems, it is difficult to discern the exact details of G protein-mediated effects, as the identity of all the components in the signaling complex and the functional state of each participating component are not known. Third, no direct evidence has been presented from experiments with Kir3 channels for stimulatory effects in the co-presence of both active G protein subunits. The requirement for an activated Gαs subunit has been demonstrated in the Gβγ stimulation of certain adenylyl cyclase isoforms (57, 58). Thus, these new findings with the Kir3.1 chimera will need to be compared explicitly with Kir3 channels expressed in cell and cell-free systems.

Perhaps the greatest un-reconciled difference in the results obtained between prior experiments with Kir3 channels expressed in cellular systems and the present ones carried out with purified components in planar lipid bilayers is that cell-free patches apparently respond to Gβγ subunits without the need for concurrent Gα activation. Yet, one can imagine that

if endogenous G protein-coupled receptors were part of the signaling complex (missing in our bilayer reconstitution experiments), they might cause partial G protein subunit activation through their basal and agonist-independent activity. In such a scenario, $G\beta\gamma$ stimulation could be coupled to a concurrent $G\alpha$ activation for stimulation of Kir3 currents. Alternatively, the replacement of the Kir3.1 transmembrane domains by the corresponding KirBac1.3 region and/or the lack of the last 129 amino acid residues of Kir3.1 could be responsible for this difference. These and other predictions born out from the present experiments with the Kir3.1 chimera model will undoubtedly stimulate new experiments with Kir3 channels expressed in native and heterologous cell systems, as well as in planar lipid bilayers.

To date, progress in structural studies of Kir3-$G\beta\gamma$ complexes has been hampered in part by the fact that even though crystal structures of $G\beta\gamma$ dimers exist (*e.g.*, Ref. 59) "functional" Kir3 channels of known structures had not been reported. Various crystallographic studies have provided structural information on Kir3 channels. Two of them lacked the transmembrane region describing the soluble cytoplasmic pores of eukaryotic Kir3.1 and Kir3.2 at 1.8 and 2.3Å, respectively (18, 20). The third one, the Kir3.1 chimera at 2.2Å, provided the Kir3.1 cytosolic pore in the context of a prokaryotic transmembrane domain (17). We believe that our single-particle electron microscopy work on the Kir3.1 chimera paves the way for structural studies of Kir3.1 chimera-$G\beta\gamma$ complexes using hybrid approaches (53), based on the fitting of existing crystal structures of the individual components to three-dimensional electron microscopy maps. Together with other structural approaches, such as x-ray crystallography and computational chemistry, structural models of complexes between Kir3 channels and G proteins will allow a greater in depth study of G protein regulation of effectors.

The present studies suggest that both G protein subunits are critically involved in the regulation of the activity of the Kir3.1 chimera. Thus it is important that future studies aim to discern the structural interrelationships of the entire signaling complex, which may confer the stability necessary for successful structural studies.

Acknowledgments—We thank Motohiko Nishida and Roderick MacKinnon for sharing the Kir3.1 chimera construct. We are also grateful to Dr. James Wells (University of Toronto) for useful discussions, Dr. David Stokes (New York University) for constructive feedback on the manuscript, and members of the Logothetis and Ubarretxena laboratories for helpful discussions throughout the project. We also thank the New York Structural Biology Center for use of its electron microscopy facilities.

REFERENCES

1. Huang, C. L., Feng, S., and Hilgemann, D. W. (1998) *Nature* **391,** 803–806
2. Sui, J. L., Petit-Jacques, J., and Logothetis, D. E. (1998) *Proc. Natl. Acad. Sci. U.S.A.* **95,** 1307–1312
3. Logothetis, D. E., Lupyan, D., and Rosenhouse-Dantsker, A. (2007) *J. Physiol.* **582,** 953–965
4. Logothetis, D. E., Kurachi, Y., Galper, J., Neer, E. J., and Clapham, D. E. (1987) *Nature* **325,** 321–326
5. Reuveny, E., Slesinger, P. A., Inglese, J., Morales, J. M., Iñiguez-Lluhi, J. A., Lefkowitz, R. J., Bourne, H. R., Jan, Y. N., and Jan, L. Y. (1994) *Nature* **370,** 143–146
6. Yamada, M., Innabe, A., and Kurachi, Y. (1998) *Pharmacol. Rev.* **50,** 723–760
7. Hibino, H., Inanobe, A., Furutani, K., Murakami, S., Findlay, I., and Kurachi, Y. (2010) *Physiol. Rev.* **90,** 291–366
8. Stanfield, P. R., Nakajima, S., and Nakajima, Y. (2002) *Rev. Physiol. Biochem. Pharmacol.* **145,** 47–179
9. Kubo, Y., Reuveny, E., Slesinger, P. A., Jan, Y. N., and Jan, L. Y. (1993) *Nature* **364,** 802–806
10. Dascal, N., Lim, N. F., Schreibmayer, W., Wang, W., Davidson, N., and Lester, H. A. (1993) *Proc. Natl. Acad. Sci. U.S.A.* **90,** 6596–6600
11. Lesage, F., Duprat, F., Fink, M., Guillemare, E., Coppola, T., Lazdunski, M., and Hugnot, J. P. (1994) *FEBS Lett.* **353,** 37–42
12. Krapivinsky, G., Gordon, E. A., Wickman, K., Velimirović, B., Krapivinsky, L., and Clapham, D. E. (1995) *Nature* **374,** 135–141
13. Tao, X., Avalos, J. L., Chen, J., and MacKinnon, R. (2009) *Science* **326,** 1668–1674
14. Doyle, D. A., Cabral, J. M., Pfeutzner, R. A., Kuo, A., Gulbis, J. M., Cohen, S. L., Chait, B. T., and Mackinnon, R. (1998) *Science* **280,** 69–77
15. Kuo, A., Gulbis, J. M., Antcliff, J. F., Rahman, T., Lowe, E. D., Zimmer, J., Cuthbertson, J., Ashcroft, F. M., Ezaki, T., and Doyle, D. A. (2003) *Science* **300,** 1922–1926
16. Kuo, A., Domene, C., Johnson, L. N., Doyle, D. A., and Vénien-Bryan, C. (2005) *Structure* **13,** 1463–1472
17. Nishida, M., Cadene, M., Chait, B. T., and MacKinnon, R. (2007) *EMBO J.* **26,** 4005–4015
18. Nishida, M., and MacKinnon, R. (2002) *Cell* **111,** 957–965
19. Pegan, S., Arrabit, C., Zhou, W., Kwiatkowski, W., Collins, A., Slesinger, P. A., and Choe, S. (2005) *Nat. Neurosci.* **8,** 279–287
20. Inanobe, A., Matsuura, T., Nakagawa, A., and Kurachi, Y. (2007) *Channels* **1,** 39–45
21. Mirshahi, T., and Logothetis, D. E. (2004) *J. Biol. Chem.* **279,** 11890–11897
22. Lesage, F., Guillemare, E., Fink, M., Duprat, F., Heurteaux, C., Fosset, M., Romey, G., Barhanin, J., and Lazdunski, M., (1995) *J. Biol. Chem.* **270,** 28660–28667
23. Chan, K. W., Sui, J. L., Vivaudou, M., and Logothetis, D. E. (1996) *Proc. Natl. Acad. Sci. U.S.A.* **93,** 14193–14198
24. Vivaudou, M., Chan, K. W., Sui, J. L., Jan, L. Y., Reuveny, E., and Logothetis, D. E. (1997) *J. Biol. Chem.* **272,** 31553–31560
25. Logothetis, D. E., Petrou, V. I., Adney, S. K., and Mahajan, R. (2010) *Pflugers Arch.* **460,** 321–341
26. Logothetis, D. E., and Nilius, B. (2007) *Pflügers Arch.* **455,** 1–3
27. Logothetis, D. E., Jin, T., Lupyan, D., and Rosenhouse-Dantsker, A. (2007) *Pflügers Arch.* **455,** 83–95
28. Stansfeld, P. J., Hopkinson, R., Ashcroft, F. M., and Sansom, M. S. (2009) *Biochemistry* **48,** 10926–10933
29. Lopes, C. M., Zhang, H., Rohacs, T., Jin, T., Yang, J., and Logothetis, D. E. (2002) *Neuron* **34,** 933–944
30. Ludtke, S. J., Baldwin, P. R., and Chiu, W. (1999) *J. Struct. Biol.* **128,** 82–97
31. Marabini, R., Masegosa, I. M., San, Martin, M. C., Marco, S., Fernandez, J. J., de, la, Fraga, L. G., Vaquerizo, C., and Carazo, J. M. (1996) *J. Struct. Biol.* **116,** 237–240
32. Scheres, S. H., Núñez-Ramírez, R., Sorzano, C. O., Carazo, J. M., and Marabini, R. (2008) *Nat. Protoc.* **3,** 977–990
33. Mindell, J. A., and Grigorieff, N. (2003) *J. Struct. Biol.* **142,** 334–347
34. Heymann, J. B. (2001) *J. Struct. Biol.* **133,** 156–169
35. Scheres, S. H., Núñez-Ramírez, R., Gómez-Llorente, Y., San, Martín, C., Eggermont, P. P., and Carazo, J. M. (2007) *Structure* **15,** 1167–1177
36. Leal-Pinto, E., London, R. D., Knorr, B. A., and Abramson, R. G. (1995) *J. Membr. Biol.* **146,** 123–132
37. Leal-Pinto, E., Tao, W., Rappaport, J., Richardson, M., Knorr, B. A., and Abramson, R. G. (1997) *J. Biol. Chem.* **272,** 617–625
38. Rostovtseva, T. K., Kazemi, N., Weinrich, M., and Bezrukov, S. M.

(2006) *J. Biol. Chem.* **281,** 37496–37506
39. Pettersen, E. F., Goddard, T. D., Huang, C. C., Couch, G. S., Greenblatt, D. M., Meng, E. C., and Ferrin, T. E. (2004) *J. Comput. Chem.* **25,** 1605–1612
40. Rubinstein, J. L. (2007) *Methods* **41,** 409–416
41. Muench, S. P., Huss, M., Song, C. F., Phillips, C., Wieczorek, H., Trinick, J., and Harrison, M. A. (2009) *J. Mol. Biol.* **386,** 989–999
42. Chan, K. W., Langan, M. N., Sui, J. L., Kozak, J. A., Pabon, A., Ladias, J. A., and Logothetis, D. E. (1996) *J. Gen. Physiol.* **107,** 381–397
43. Rohács, T., Chen, J., Prestwich, G. D., and Logothetis, D. E. (1999) *J. Biol. Chem.* **274,** 36065–36072
44. Jin, W., and Lu, Z. (1998) *Biochemistry* **37,** 13291–13299
45. Jin, W., Klem, A. M., Lewis, J. H., and Lu, Z. (1999) *Biochemistry* **38,** 14294–14301
46. Jin, W., and Lu, Z. (1999) *Biochemistry* **38,** 14286–14293
47. Aryal, P., Dvir, H., Choe, S., and Slesinger, P. A. (2009) *Nat. Neurosci.* **12,** 988–995
48. Kobayashi, T., Ikeda, K., Kojima, H., Niki, H., Yano, R., Yoshioka, T., and Kumanishi, T. (1999) *Nat. Neurosci.* **2,** 1091–1097
49. Lewohl, J. M., Wilson, W. R., Mayfield, R. D., Brozowski, S. J., Morrisett, R. A., and Harris, R. A. (1999) *Nat. Neurosci.* **2,** 1084–1090
50. He, C., Zhang, H., Mirshahi, T., and Logothetis, D. E. (1999) *J. Biol. Chem.* **274,** 12517–12524
51. He, C., Yan, X., Zhang, H., Mirshahi, T., Jin, T., Huang, A., and Logothetis, D. E. (2002) *J. Biol. Chem* **277,** 6088–6096
52. Aleksandrov, A., Velimirovic, B., and Clapham, D. E. (1996) *Biophys. J.* **70,** 2680–2687
53. Schreibmayer, W., Dessauer, C. W., Vorobiov, D., Gilman, A. G., Lester, H. A., Davidson, N., and Dascal, N. (1996) *Nature* **380,** 624–627
54. Rubinstein, M., Peleg, S., Berlin, S., Brass, D., and Dascal, N. (2007) *J. Physiol.* **581,** 17–32
55. Ikeda, S. R. (1996) *Nature* **380,** 255–258
56. Herlitze, S., Garcia, D. E., Mackie, K., Hille, B., Scheuer, T., and Catterall, W. A. (1996) *Nature* **380,** 258–262
57. Tang, W. J., and Gilman, A. G. (1991) *Science* **254,** 1500–1503
58. Gao, B. N., and Gilman, A. G. (1991) *Proc. Natl. Acad. Sci. U.S.A.* **88,** 10178–10182
59. Gaudet, R., Bohm, A., and Sigler, P. B. (1996) *Cell* **87,** 577–588